Materials and Structures
DOI 10.1617/s11527-014-0328-1

ORIGINAL ARTICLE

Imaged-based discrete element modeling of hot mix asphalt mixtures

Mohammad J. Khattak · Ahmed Khattab · Hashim R. Rizvi · Subasish Das · Mohammad R. Bhuyan

Received: 7 April 2013 / Accepted: 2 May 2014

Abstract This paper presents the development of micro-mechanical discrete element model for hot mix asphalt (HMA) mixtures modified with carbon nanofibers using the advanced imaging techniques. Shape-structural model of two-phased HMA consisting of aggregate and matrix was generated using cluster of small discrete disk-shaped particles for each phase. Three contact models, shear and normal stiffness, static and sliding friction, and inter-particle contact bonds were employed to model the constitutive behavior of the HMA mixture. To validate the developed DEM model an experimental study was executed. It was observed that the uniaxial compressive test simulation reasonably predicted the stress–strain behavior of the HMA mixture. The dynamic modulus and strength obtained from indirect tensile test were similar to the predicted moduli and strength using the DEM under the quasi-elastic state for all the HMA mixtures studied.

Keywords Micro-mechanical model · PFC^{2D} · HMA · Compressive strength · Discrete element model · Constitutive behavior · Carbon nanofibers

M. J. Khattak (✉) · H. R. Rizvi · S. Das · M. R. Bhuyan
Department of Civil Engineering, University of Louisiana at Lafayette, Lafayette, LA, USA
e-mail: khattak@louisiana.edu

H. R. Rizvi
e-mail: hrr9588@louisiana.edu

S. Das
e-mail: sxd1684@louisiana.edu

M. R. Bhuyan
e-mail: buet_reza@yahoo.com

A. Khattab
Department of Industrial Technology, College of Engineering, University of Louisiana at Lafayette, Lafayette, LA, USA
e-mail: khattab@louisiana.edu

Published online: 09 May 2014

1 Introduction and background

Hot mix asphalt mixtures (HMA) are usually modeled using a continuum mechanics approach. However, in reality, the HMA mixture consists of asphalt binder, coarse and fine aggregates and air voids. Most of the damage occurs in asphalt binder and microstructure of aggregate skeleton. HMA mixture mechanistic properties are dependent on the fundamental characteristics of the three components of the mixtures. Therefore, basic knowledge of micro-structural behavior related to stress transmission, stress intensities and micro damage in the aggregate structure and asphalt matrix need special attention.

Various researchers have utilized the finite element and discreet element to understand the mechanical behavior of HMA mixtures [1–9]. Finite element modeling of the HMA can create adequate

microstructure geometry of aggregate and mastic. However, current approach has limitations in its convergence difficulties in modeling the changes in the aggregate contact geometry, aggregates coming in and out of contact and sliding during loading. Additionally, the modeling of aggregate or mastic fracture behavior during strength test simulations is very cumbersome. Such difficulties are normally overcome by using continuum approach, in such case the microstructural features are neglected and homogenized into an equivalent material [9].

The discrete element modeling (DEM) was introduced by Cundall [10] for analysis of rock mechanics, and successfully applied to granular materials (soils) [11] and solid materials with bonded contact models [12]. DEM is a numerical technique, in which Newton's second law of motion and a finite difference scheme are utilized to study the interaction among discrete particles in contact [12]. Amongst various discrete elements codes the particle flow code $(PFC)^{2D}$ has higher computation efficiency and the ability to model fracture behavior, interaction, as well as the interface conditions (adhesion) between the various phases of HMA materials [5, 12]. DEM has been utilized by Buttlar et al. [5] to predict the creep strain of an HMA laboratory tested sample. The computer software PFC^{2D} was implemented to model the contact and displacement of disk- shaped discrete element particles used to construct DEM of mastic. Although the models were limited to a 2D analysis they were able to predict the mastic mixture properties reasonably well [4–6]. Similar technique was applied to determine the HMA mixture complex modulus at −20 °C [6]. In this technique, aggregate and matrix phases of HMA were modeled by cluster of finite disk-shaped particles. By modeling the aggregate and matrix with a mesh of small disk-shaped particles called ''microfabric,'' it was possible to model complex aggregate shapes. Such modeling technique was later adopted by Khattak and Roussel [13] to predict the dynamic modulus of HMA mixture under indirect tension mode. Abbas [7] has successfully modeled asphalt mastic and HMA mixtures using DEM. Asphalt mastic (asphalt and fines passing 0.075 mm sieve) was simulated using an assembly of stiff particles randomly dispersed in a medium of soft particles, representing the aggregate fillers and the asphalt binder, respectively. These mastic models were used to simulate the micromechanical behavior of HMA mixtures tested under simple performance test and indirect test conditions. Adhikari and You [8] used X-ray computed tomography (X-ray CT) images to characterize the aggregate orientation, aggregate gradation, sand mastic, and air void distribution in the asphalt mixture. It was found that the modulus values using 3D model were better than the predictions made from 2D model and compared well with the laboratory measured HMA moduli. Although, 3D model predicted fairly well the moduli values, the time and effort in processing, not to mention the computing time for simulation are significant. Liu and You [14] developed DEM viscoelastic model to study the effect of the aggregate sphericity, fractured faces, and orientation on the creep stiffness of HMA mixtures. It was found that the HMA creep stiffness increases with increase in aggregate sphericity and orientation. However, the effect of aggregate fracture faces was not significant. Chen et al. [15] simulated the compaction of HMA mixtures and evaluated the aggregate gradation, gyration number and gyration angle. The results showed that the DEM compaction simulation was in agreement with the laboratory compaction data. Mahmoud et al. [16] investigated the effect of aggregate gradation, shape characteristics, and strength on HMA strength and stiffness using the image-based DEM. Their developed model effectively demonstrated the impact of the variability of aggregate characteristics, aggregate blending, and the distribution of the internal structure on HMA mixture response.

Even though good progress has been made by a number of researchers, the understanding of the micromechanics behavior of the HMA mixture is still not fully understood. Most of the aforementioned studies concentrated in evaluating the stiffness/moduli and effect of aggregate characteristics on response of the HMA mixture using micromechanical approach. The development of a micromechanical model to predict HMA properties such as strength and moduli/stiffness is still very necessary to not only validate the previous studies but also to further understand the micro-level responses of HMA mixtures. In this study, the developed model determines the complete stress strain response of HMA mixtures with the capability to relate the changes in the asphalt matrix characteristics, due to carbon nanofibers (CNF) modification, to the strength and stiffness of the mixture. This paper presents the

Table 1 Aggregate gradation data

Sieve Sizes	US (inch) Metric (mm)	¾″ 19	½″ 12.5	3/8″ 6.25	No. 4 4.75	No. 10 2.0	No. 40 0.425	No. 80 0.18	No. 200 0.075
% Passing	HMA	100	92	85	62	41	21	13	2
	AM	–	–	–	–	100	51.2	31.7	4.9

application of microfabric micromechanical DEM to model the mechanical response of neat and CNF modified HMA mixtures due to applied load. Micromechanical parameters required to develop DEM were determined from the mechanical characteristic obtained using laboratory experiments. Advanced imaging techniques were utilized to capture the actual shape and distribution of aggregate in HMA mixture. The digital image was than transformed to build a synthetic shape-structural model to help develop constitutive model of HMA mixture using the PFC^{2D} code. The developed micromechanical DEM was utilized to determine the strength, and dynamic modulus of the HMA mixtures using quasi-elastic approach.

2 Objectives of the study

The main objectives of the study are as follows:

1. Develop 2D micromechanical model of HMA and asphalt matrix (AM) mixtures using the DEM PFC^{2D} and advanced imaging techniques to simulate the strength and modulus characteristics of the HMA mixtures.
2. Conduct a laboratory investigation to compare the laboratory dynamic modulus and strength of neat and CNF modified HMA mixtures under indirect tension mode to the results of DEM simulations.

3 Test materials and methods

3.1 Materials

Three types of the HMA and AM mixtures were constructed using the limestone aggregate, viscosity graded AC5 and carbon nanofibers (CNF). (1) AC5–neat mixtures—the mixtures made using neat asphalt binders, (2) AC5–1.5 % CNF mixtures—the mixtures made using 1.5 % CNF modified asphalt. (3) AC5–6.5 % CNF mixtures—the mixture made using 1.5 % CNF modified asphalt and 5 % CNF as particle additive in aggregate.

Superpave design procedure was used to construct HMA mixtures. The nominal maximum aggregate size of 19 mm was used with an optimum asphalt binder content of 4.0 %. For 6.5 % CNF HMA mixtures, adjustment in fines was also made to accommodate the CNF. The cylindrical HMA samples of 150 mm diameter were compacted by the Superpave Gyratory Compactor, and then sliced using the diamond saw to obtain 32 mm thick specimens. Table 1 shows the aggregate gradations for both the AM and HMA mixtures. The AM mixtures were made using 9.2 % of asphalt binder and fine aggregate passing No. 10 sieve. The aggregate gradation for AM was extracted from HMA mixture gradation (Table 1). The sample dimensions were 9.5 mm in diameter, and 9.5 mm in height for dynamic shear modulus (DSR) testing. A detailed description of AM sample preparation and molding can be found elsewhere [17]. Triplicate specimens were constructed for both HMA and AM mixtures and following mechanical tests were conducted.

3.2 Dynamic modulus (E^*) of HMA mixtures

HMA specimens were subjected to indirect tensile (IDT) cyclic loading at test temperature of 25 °C. Testing was performed using a closed-loop servo-hydraulic machine, manufactured by material testing system (MTS). The E^* test protocol as suggested by Kim et al. [18] with slight modification was used. The mixtures were tested at frequencies of 25, 5, and 1 Hz under stress control mode within the linear visco-elastic stress range. Indirect tensile loading was applied, and the strain was measured by using surface mounted miniature linear voltage differential transducers (LVDT) in the horizontal and vertical directions on both sides of the HMA specimen. The gauge length was kept at 50.8 mm. In order to ensure that the testing was performed within the linear visco-elastic

stress range the horizontal strains were kept between 80 and 100 μm throughout the testing. The following equation derived by Kim [14] was used to calculate the E^* under IDT of HMA.

$$E^* = \frac{2 \cdot P}{\pi \cdot a \cdot d}\left[\frac{\beta_1 \cdot \gamma_2 - \beta_2 \cdot \gamma_1}{\gamma_2 \cdot D_V - \beta_2 \cdot D_H}\right], \quad (1)$$

where, P applied load, N; a loading strip width, m; d thickness of specimen, m; D_V vertical deformation, m; D_H horizontal deformation, m; and β_1, β_2, γ_1 and γ_2 are coefficients and are equal to −0.0202307, −0.0062774, 0.0054818, and 0.0174723, respectively. These values are based on the loading strip width of 19 mm, diameter of 150 mm and gauge length of 50.8 mm.

3.3 Indirect tensile test of HMA mixtures

Indirect tensile test was performed on the same specimen as the dynamic modulus test. Initially, the specimen was allowed to recover some deformation that had occurred during the dynamic modulus test. A ramp loading at a constant rate of 5.1 cm/min was applied until failure. The magnitude of the load and the deformations in the mixture in both vertically and horizontally were measured. Indirect tensile strength (ITS) and compressive strength (ICS) values were calculated using the following equations.

$$\text{ITS} = \frac{2 \cdot P}{\pi \cdot D \cdot t} \quad (2)$$

$$\text{ICS} = \frac{6 \cdot P}{\pi \cdot D \cdot t}, \quad (3)$$

where, P load at failure, D diameter of specimen and t thickness of the specimen.

3.4 Mechanical testing of AM mixtures

3.4.1 Complex shear modulus (G^*)

A frequency sweep test was conducted to determine the complex shear modulus (G^*) of AM using the Bholin's dynamic shear rheometer (DSR). All testing were conducted on triplicate samples of AM at 25 °C. The AM sample (9.5 mm diameter and 9.5 mm thick) was glued to the top and bottom plate of DSR. The sample was subjected to various loading frequency levels, from 1 to 60 Hz at logarithmic increments in a controlled stress mode. Prior to testing, a stress sweep was applied at to determine the visco-elastic stress limits. The visco-elasticity holds if the decrease in G^* of the AM was within 10 % [17]. Once the maximum stress limits were established, the actual samples were tested at 90 % of maximum stress level. The samples were also conditioned before each test for 100 cycles at 10 Hz, at half the actual stress used for testing.

3.4.2 Direct tension test

The tensile strength of AM mixture was determined using the test method, described in AASHTO T132 with slight modification. Normally, it involves the direct tension testing of a small briquette samples. The dogbone-shaped briquette is 76 mm long and has a 645 mm^2 cross-section at mid length. Special self-aligning grips allowed passive gripping of the specimen in the test machine and ensured uniform loading. Traditionally, the test is conducted in load-controlled mode. However, in this study a strain control mode of loading was applied at a rate of 5.1 cm/min. Triplicate samples of AM were tested at 25 °C. For determining the bond strength at the interface of aggregate and AM, an aggregate cube (25 mm × 25 mm × 25 mm) was placed in the dogbone mold just before compacting the AM into the mold as shown in Fig. 1. The AM-aggregate specimens were tested as described above at the end of the curing period.

The tensile strength and bond strength were calculated using the following equation.

$$\sigma_t = \frac{P_t}{A}, \quad (4)$$

where, σ_t tensile/bond strength, P_t tensile load at failure, A cross-sectional area on which tensile load is

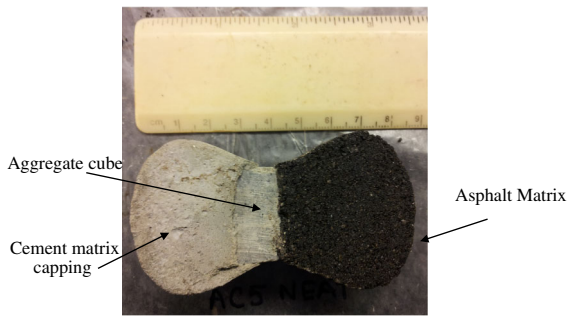

Fig. 1 Dogbone sample for bond strength determination of AM–aggregate interface

applied. The tensile and bond strengths, obtained from Eq. 4, were used to determine the micromechanical normal bond properties of AM mixtures and AM-Aggregate interface for DEM as explained in Sect. 4.0.

3.4.3 Uniaxial compression test

This test was conducted similar to ASTM C39 test method. A 25 mm in diameter by 50 mm high AM sample was loaded at an axial strain rate of 5.1 cm/min until failure using the material testing system (MTS). Real time data acquisition was performed and time, load and deformations were recorded. This facilitated in capturing the complete stress -strain response of the samples. Three AM samples were tested under compression loading. The compressive strength was calculated using the following equation.

$$\sigma_c = \frac{P_c}{A}, \tag{5}$$

where, σ_c compressive strength, P_c compressive load at failure, A cross-sectional area on which compressive load is applied.

3.4.4 Direct shear test

The shear strength of AM mixture was determined by applying direct shear load on 62.5 mm diameter and 25 mm thick AM sample. A shear rate of 5.1 cm/min was applied until failure using the MTS as shown in Fig. 2. A strap belt was also applied at the top of the sample to hold the sample in place without pulling out due to shear load.

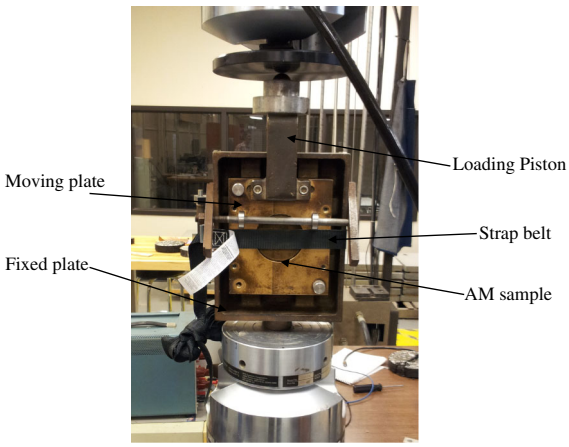

Fig. 2 Direct shear test assembly for AM mixtures

$$\tau = \frac{P_s}{A_s}, \tag{6}$$

where, τ shear strength, P_s shear load at failure, A_s cross-sectional area on which shear load is applied

4 Micro-mechanical discrete element model

4.1 Contact stiffness and bonds constitutive models

In the DEM approach, shear and normal stiffness, static and sliding friction, and inter-particle contact bonds (cohesion/adhesion) are three contact models, which are employed to establish the micromechanical constitutive behavior of the material. Figure 3 illustrates two particles A and B in contact, where normal stiffnesses are shown to have magnitudes k_n^A and k_n^B, and shear stiffnesses have magnitudes of k_s^A and k_s^B, respectively. For a linear contact model, the contact stiffness is computed by assuming that the stiffnesses of the two contacting particles act in series. The force–displacement law of the two particles in contact can be expressed using the following set of equations [12].

$$F_n = n \cdot K_n \cdot U_n \tag{7}$$

$$\Delta F_s = -k_s \cdot \Delta U_s \tag{8}$$

$$K_n = \frac{k_n^A \cdot k_n^B}{k_n^A + k_n^B} \tag{9}$$

$$K_s = \frac{k_s^A \cdot k_s^B}{k_s^A + k_s^B} \tag{10}$$

4.2 Micro-mechanical model parameters

The micro-mechanical parameters used for modeling are derived from macro-mechanical characteristics of the materials. In general, the macro properties such as elastic modulus and strengths for each component of the composite materials are either determined in the laboratory or obtained from the manufacturer. Once the macro properties are known the micro parameters are calculated using the following set of equations [12]:

$$k_n = 2Et \quad \text{and} \quad k_s = 2Gt \tag{11}$$

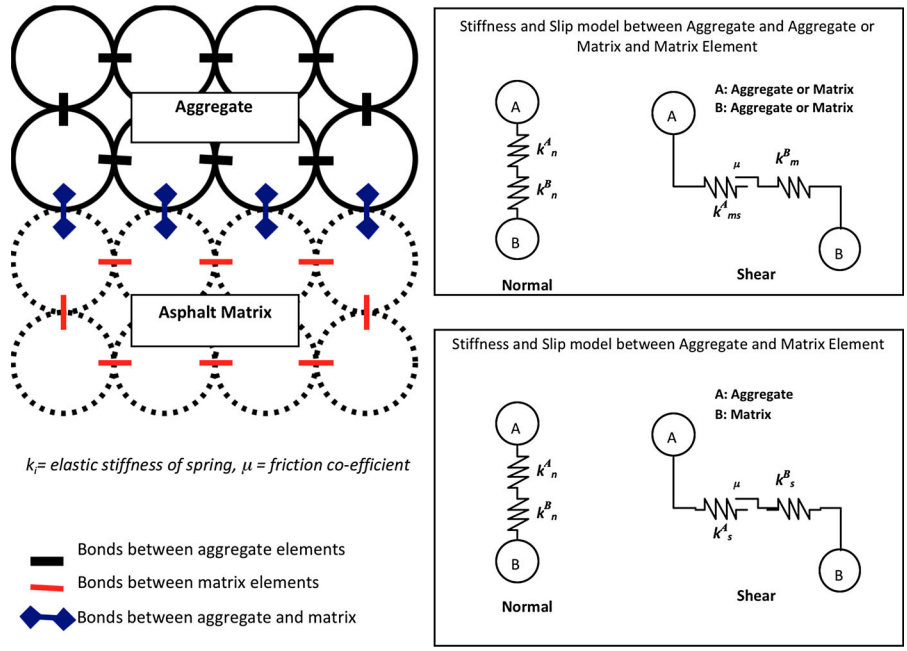

Fig. 3 Schematic of contact and bond models

$$G = \frac{E}{2(1+v)} \tag{12}$$

$$S_n = 2\sigma_t Rt \quad \text{and} \quad S_s = 2\tau_o Rt, \tag{13}$$

where E and G are the elastic and shear moduli, respectively; the σ_t and τ_o are the tensile and shear strengths, respectively; v is the Poisson ratio, R is the radius of particle (disk) and t is the thickness of particle (unit thickness is used). The contact bonds are characterized as point forces in normal (S_n) direction and shear (S_s) direction. Section 3.4 demonstrates the mechanical tests that were used to determine the tensile and shear strengths.

The micro-scale model parameters for parallel bond used to simulate cementation effect (adhesion) are normal and shear stiffnesses $\left(k_{pn}^{A}, k_{ps}^{A}, k_{pn}^{B}, k_{ps}^{B}\right)$, normal and sheer strengths (σ_{pt} and τ_{po}), and radius of the parallel bond (R_p).

$$k_{pn,ps} = \frac{k_{n,s}}{A_p} = \frac{k_{n,s}}{L_p t} = \frac{k_{n,s}}{2(\overline{R})t} \tag{14}$$

where, $\overline{R}$ mean radius of two contact elements; L_p length of the parallel bond; and R_p = radius of parallel bond, a maximum value of 1 indicates that the parallel bond (cementation effect) extends to the mean diameter of the two contact elements.

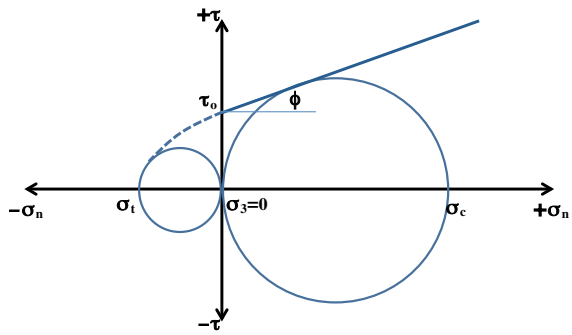

Fig. 4 Determination of angle of internal friction (ϕ)

The coefficient of friction (μ) is assumed to be the function of the angle of internal friction (ϕ) of each component of the material and is determined as:

$$\mu = \tan(\phi) \tag{15}$$

Knowing the laboratory tensile strength (σ_t), shear strength (τ_o) and compressive strength (σ_c) at confining strength (σ_3) of zero, the ϕ value can be determined using the Mohr–Coulomb failure envelop represented by Eq. 16 and shown in the Fig. 4.

$$\tau = \tau_o + \sigma_n \tan(\phi) \tag{16}$$

Murrell [19] suggested that the brittle fracture criterion proposed by Griffith [20, 21] could be applied to rocks. Griffith's theory was originally derived for

tensile stress fields. In order to apply this criterion to rocks and similar materials subjected to compressive stress conditions, the frictional strength of closed crack has to be allowed for, which was proposed by McClintock and Walsh [22]. The Mohr failure envelope for the modified Griffith theory is then defined by the equation:

$$\tau = 2\sigma_t + \sigma_n \tan(\phi) \quad (17)$$

Comparison of Eqs. 16 and 17 suggests that the shear bond strength or cohesion of the material equals twice the tensile strength of the material ($\tau_o = 2\sigma_t$). Hence, the ϕ value can be determined in two ways:

1. Experimentally determine the τ_o and σ_c at $\sigma_3 = 0$ and plot the values on $\tau - \sigma_n$ plane as shown in Fig. 4. The slope of the line with origin at τ_o and tangent to the Mohr circle for σ_c is the ϕ value of the material.
2. Experimentally determine σ_t and σ_c at $\sigma_3 = 0$ and plot the values on $\tau - \sigma_n$ plane as shown in Fig. 4. Locate the $\tau_o = 2\sigma_t$ on τ-axis. The slope of the line with origin at $\tau_o = 2\sigma_t$ and tangent to the Mohr circle for σ_c is the ϕ value of the material.

Based on the above discussion, the micro-mechanical normal bond (S_n) and shear bond (S_s) strengths and coefficient of friction (ϕ) for each component (aggregate and matrix) of HMA mixture can be determined using Eqs. 13 and 15 for DEM constitutive modeling of HMA mixtures.

4.3 Image-based shape-structural model

The cut specimens of HMA specimen using the diamond saw was thoroughly surface cleaned using water and allowed to air dry at room temperature. The specimen was than scanned to obtain a digital image of the cross-sectional area as shown in Fig. 5. The specimen image was trimmed to a 25 mm × 50 mm sized image for processing and developing a synthetic PFC^{2D} model. A black and white digital image was generated that would interpret matrix and aggregate phases, respectively. The digital image was processed through a routine developed in C^{++} programming to establish a numerical logical matrix of the digital image identifying aggregate and matrix pixels. The developed routine established x- and y-coordinates for aggregate and matrix particles. Such routines also used to create the consistent coding for PFC^{2D} with appropriate disk-shaped particle radii, heights, widths as well as identification of interface particles (adhesive bonds) between matrix and aggregate. Finally, a heterogeneous synthetic HMA image-based shape-structural model was developed after executing PFC^{2D} as shown in Fig. 5. A portion of the synthetic model was also zoomed-in for details of aggregate and matrix particles.

5 Results and discussion

5.1 DEM simulations using PFC^{2D}

The micro-mechanical properties derived from macro-properties (Table 2) obtained from the laboratory experiments used for the DEM model are shown in Table 3. The aggregate mechanical properties including elastic modulus (E), modulus of rapture (Sr) and Poisson's ratio (v) were obtained from the manufacturer. However, for AM mixtures the mechanical characteristics were obtained from laboratory experiments as described earlier. The complex shear moduli (G^*) of AM were used to calculate dynamic moduli (E^*) by utilizing Eq. 12. The Poisson's ratio of HMA mixture is of the range 0.30–0.35, however, the AM mixtures are softer than the HMA mixtures and for such materials the v approaches 0.5 [5, 6, 13].

Initially, simple DEM were developed for AM and aggregate and elastic moduli and strengths were determined from the DEM compressive strength simulations. Each DEM model for aggregate and AM consisted of 5,000 particles with radius of 0.25 mm. Contact stiffnesses and bonds were assigned between each element. Uniaxial compressive loading was applied during the test simulation in PFC2D and the stress–strain response of the material was monitored. To determine the elastic modulus, the specimen was loaded until 150 μm-strain and then unloaded. The test simulation resulted in promising results with only 2 % error between the measured and predicted moduli values.

Once it was determined that the developed DEM model can accurately predict the moduli of aggregate and AM, the DEM for HMA mixture was developed. The synthetic model of HMA developed using imaging and PFC^{2D} as discussed above was utilized. The micromechanical properties were assigned to each component (aggregate and AM) of HMA mixture.

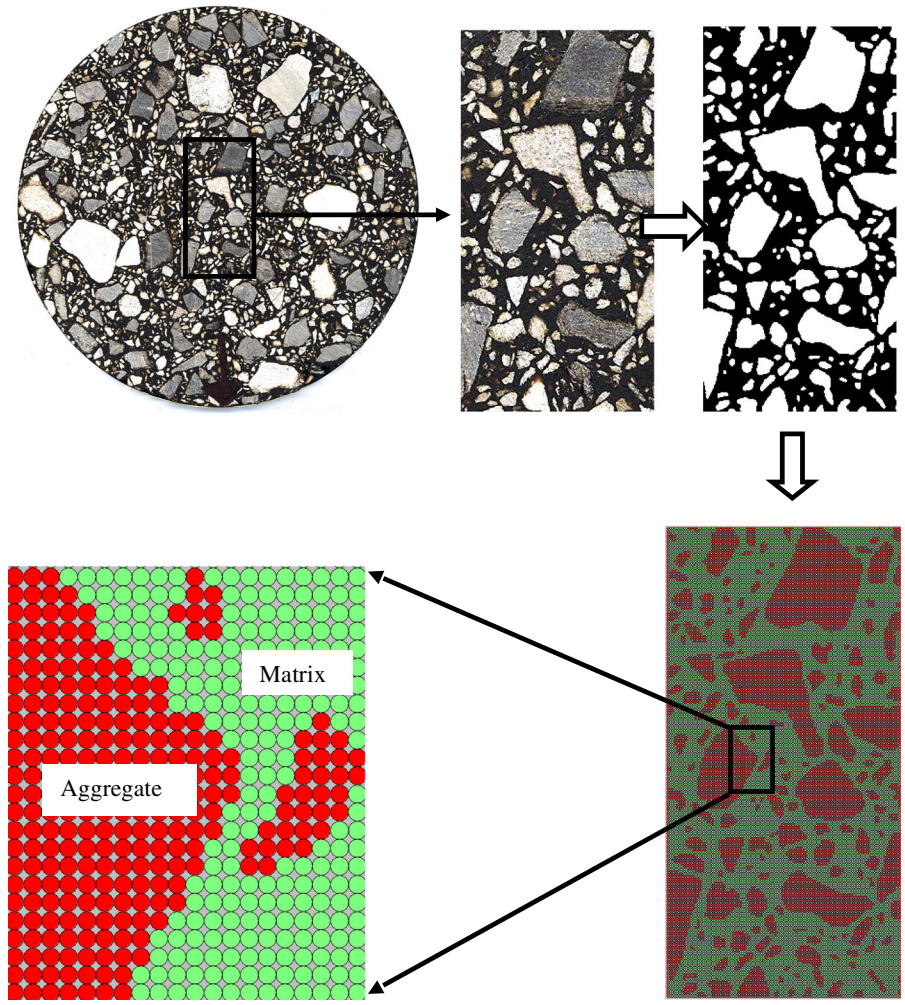

Fig. 5 Image processing and synthetic PFC^{2D} model

Contact stiffness and bonds were assigned to each component of HMA and parallel bonds were installed at the interface of aggregate and AM to simulate the adhesion effect at the interface. Two stiff loading plates, one at the top and one at the bottom of the synthetic specimen was placed. The top loading plate was assigned a constant rate of 0.05 m/s in compressive direction, while the bottom loading plate of the specimen was kept fixed. The average stress experienced by the plate was recorded for each loading step. Typical DEM simulation of uniaxial compressive tests is as shown in Fig. 6. Based on the scanned resolution of the image, the simulated specimens contained up to 20,000 disk-shaped particles with a radius of 0.127 mm. After a certain continuous incremental compressive loading, the response of each aggregate and each matrix particle was monitored. Figure 6a illustrates the compressive (black) and tensile (red) contact force chains as the result of the compressive test simulation in PFC^{2D}. Figure 6b demonstrates the contact force chains for the enlarged portion of Fig. 6a. Due to the heterogeneous nature of HMA mixture local tensile stresses occurred due to the applied compressive stress. Once the tensile stress exceeded the bond strength between particles the bond broke and resulted in the initiation of micro crack. These localized micro cracks interconnected together and grew into macro cracks, which further caused the complete failure of the specimen. The contact break at the interface of aggregate and matrix is also shown in Fig. 6c. The stress–strain response of the HMA synthetic model was monitor and recorded. Typical

Table 2 Average macro mechanical properties from laboratory experiments

Parameters	Aggregate	AM mixture			Aggregate–AM interface		
	Limestone	Neat	1.5 % CNF	6.5 % CNF	Limestone–neat	Limestone–1.5 %CNF	Limestone–6.5 % CNF
Elastic modulus (E) (MPa)	50,000[a]	–	–	–	–	–	–
Dynamic modulus (E^* @ 1 Hz) (MPa)	–	391	472	679	–	–	–
Modulus of rupture (Sr) (MPa)	9.2[a]	–	–	–	–	–	–
Tensile strength (σ_t) (KPa)	–	448	861	423	–	–	–
Tensile bond strength (σ_b) (KPa)	–	–	–	–	224	431	212
Compressive strength (σ_c), (Mpa)	55.1	3.1	4.5	3.0	–	–	–
Direct shear strength (τ_o) (KPa)	–	850	1,755	810	–	–	–
Angle of internal friction (ϕ)	47	30	24	30	–	–	–
Poisson's ratio (v)	0.2[a]	0.5[b]	0.5[b]	0.5[b]	–	–	–

[a] Obtained from manufacturer

[b] Assumed values (5, 6, 13)

Table 3 Average micro mechanical properties derived from macro properties

Parameters	Aggregate	AM mixture			Aggregate–AM interface		
	Limestone	Neat	1.5 % CNF	6.5 % CNF	Limestone–neat	Limestone–1.5 % CNF	Limestone–6.5 % CNF
k_n (MPa-m)	100,000	782	1,358	944	–	–	–
k_s (MPa-m)	41,667	261	453	315	–	–	–
k_{pn} (GPa-m)	–	–	–	–	3,079	5,346	3,717
k_{ps} (GPa-m)	–	–	–	–	1,026	1,782	1,239
S_n (N)	2,337	114	219	107	–	–	–
S_s (N)	4,674	216	446	206	–	–	–
σ_{pt} (Kpa)	–	–	–	–	224	431	212
τ_{po} (Kpa)	–	–	–	–	448	861	423
μ	1.1	0.60	0.50	0.55	0.60	0.50	0.55

stress–strain curve obtained from uniaxial compressive test simulation is also shown in Fig. 7 along with the laboratory test results.

5.2 Comparison of test results and DEM simulation

Figure 8 shows a typical plot of the predicted E^* and measured E^* HMA as function of the E^* of AM. As expected, the predicted moduli fall within the theoretical lower and upper bounds, but tend to be closer to the lower theoretical bound. It can be seen that with the increase of AM modulus the HMA modulus increases. While measured values of E^* are higher than the predicted ones it can be seen that the DEM model has the ability of predicting E^* trend at a given E* of AM, using its micromechanical properties.

The stiffness of the material is a function of particles in contact. Hence if the number of particles for higher stiffness material is more the overall stiffness will be more. It should be noted that various images were modeled using DEM PFC^{2D}. Based on the DEM simulations it was found that some images exhibited lower and some higher moduli values than the actual test results. Hence, aggregate volume fraction in each image was investigated. It was observed that the aggregate volume concentration for each image was different than the actual aggregate volume concentration of HMA mixture used in this study. It was found that the HMA moduli using DEM

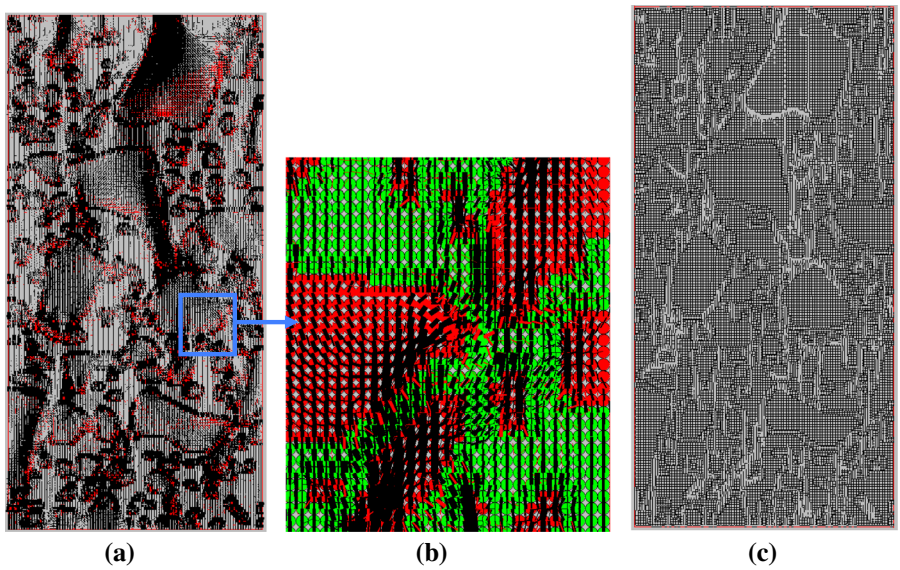

Fig. 6 Force chains of contact normal and shear forces

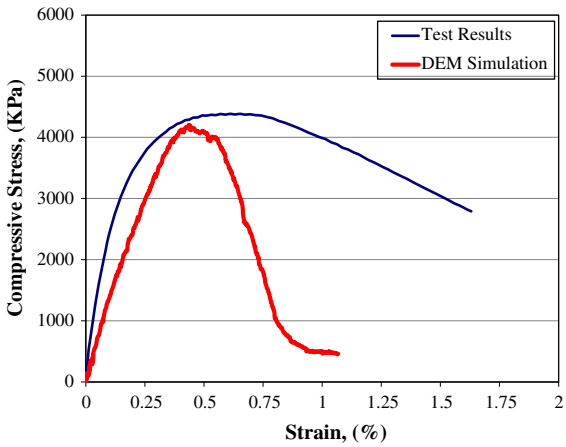

Fig. 7 Typical stress–strain response of laboratory test results and DEM simulation of AC5 Neat HMA mixtures

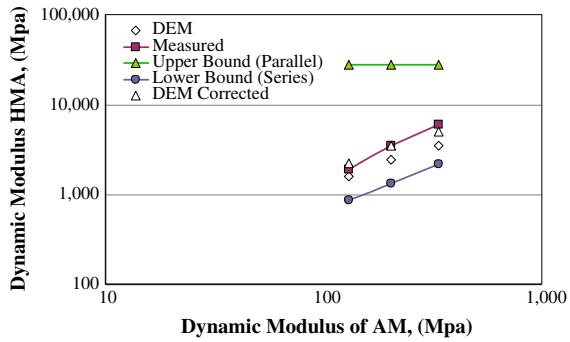

Fig. 8 Comparison of dynamic modulus predictions to theoretical bounds and experimental data for AC5 neat HMA mixtures

$\left(E_i^*\right)$ were a function of aggregate volume fraction (V_i) in an image, and modulus of AM $\left(E_{\text{am}}^*\right)$. The E_i values increases with the increase in V_i as shown in Fig. 9. Regression analysis, of DEM model modulus predictions for different images with different volume fraction, was conducted and following preliminary relationship was developed.

$$E_i^* = 1.983\left(E_{\text{am}}^*\right)^{0.787} e^{3.909(V_i)} \quad R^2 = 0.95 \text{ and } n = 54 \tag{18}$$

Based on Eq. 18 the correction factor (CF) for V_i was determined as follows:

$$\frac{E_{\text{o}}^*}{E_i^*} = \frac{1.983\left(E_{\text{am}}^*\right)^{0.787} e^{3.909(V_{\text{o}})}}{1.983\left(E_{\text{am}}^*\right)^{0.787} e^{3.909(V_i)}}$$

$$\frac{E_{\text{o}}^*}{E_i^*} = \frac{e^{3.909(V_{\text{o}})}}{e^{3.909(V_i)}}$$

$$\frac{E_{\text{o}}^*}{E_i^*} = e^{3.909(V_{\text{o}}-V_i)}$$

$$\text{CF} = e^{3.909(V_{\text{o}}-V_i)}, \tag{19}$$

where, V_{o} is aggregate volume concentration used in actual HMA mixture and E_{o} is dynamic modulus corresponding to V_{o}. In this study, V_{o} for HMA

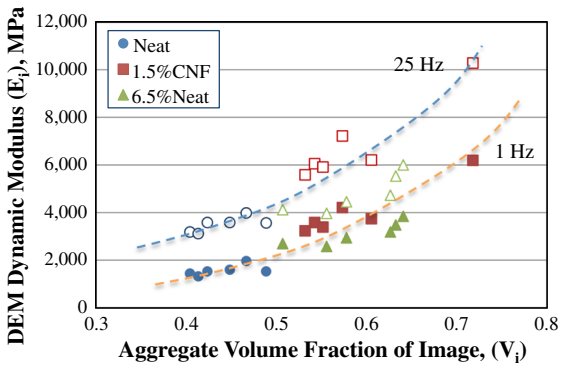

Fig. 9 Effect of aggregate volume fraction (V_i) of image on the dynamic moduli of HMA using DEM (E_i) based on E_{am} at 25 and 1 Hz

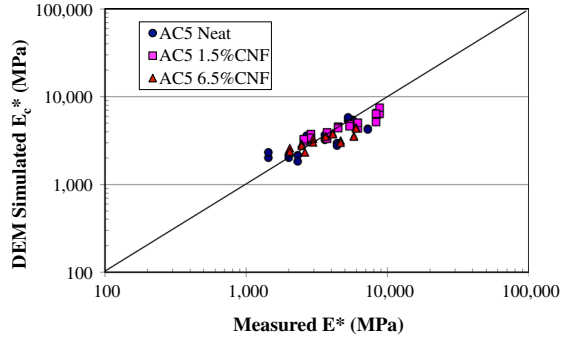

Fig. 10 Measured versus DEM simulated E^* for neat and CNF modified HMA mixture using DEM

mixture was 0.59. Hence, the corrected moduli $\left(E_c^*\right)$ are calculated using the following equation.

$$E_c^* = \mathrm{CF}(E_i^*) \tag{20}$$

The predicted E^* of HMA were adjusted using aggregate volume correction factor to better interpreted the mixture behavior s discussed above. After the correction was applied the predicted values merged with the measured values as illustrated in Fig. 10. For triplicate specimens of three HMA mixtures, tested at three loading frequencies, with two images obtained from each specimen produced 54 data points for DEM simulations. The measured and predicted E*values after corrected for aggregate volume concentration are shown in Fig. 10. It is obvious from the figure that E_c^* predictions made using the develop micromechanical DEM are reasonably well for all types of HMA mixtures used in this study. The summary of the average E^* results listed in Table 4 indicates that the difference between the actual and simulated E_c^* values ranges from 8 to 26 %. Higher differences are associated to the moduli values at higher frequency levels.

Indirect tensile strength tests were conducted on triplicate specimens of HMA mixtures. The indirect tensile and compressive strengths were determined for each mixture. Various images taken from sliced HMA specimen were used for the DEM simulations. Since, small images (25 mm × 50 mm) were used for simulations, the volume fraction and distribution of aggregate also affected the strength results. It was found that similar to E^* the compressive strength was related to the aggregate volume fraction. With the increase in the volume fraction the DEM compressive strength (S_i) of HMA mixtures increased. The following relationships were obtained using the regression analysis.

$$S_i = 287.5\left(E_{am}^*\right)^{0.536}(V_i)^{0.655}e^{-0.031(\%\ \mathrm{CNF})} \quad R^2 = 0.89 \text{ and } n = 18 \tag{21}$$

$$S_c = \mathrm{CF}(S_i) = \left(\frac{V_o}{V_i}\right)^{0.655} S_i, \tag{22}$$

where, S_i and is the compressive strength from DEM and S_c is the compressive strength corrected for aggregate volume fraction.

The strength was normalized based on the actual aggregate volume fraction of $V_o = 0.59$ for comparison purposes. Figure 11 shows the typical stress strain behavior as obtained by DEM simulations for the neat and CNF modified HMA mixtures. It can be observed that the curves for each HMA mixture are different. This implies that the developed micromechanical DEM was able to capture the effect of CNF modification of HMA. Similarly, Fig. 12 illustrates the comparison between the measured and the predicted strength values. The actual versus measured strength values are fairly well scattered along the line of equality. In general, 3–15 % of differences were noted. However, when the average values were compared the differences were reduced to 1–2.6 % (Table 5). The data in Table 5 also reveal that the measured values had up to 10 % coefficient of variation and predicted values exhibited around 8 % variation. The predicted results were within the coefficient of variation of the measured values. The prediction results are within the coefficient of

Table 4 Summary of E^* test results and DEM simulation

Mix type	Frequency (*f*)	Test results (MPa)			DEM simulation (MPa)			% Difference
		E^*	SD	CV	E_c^*	SD	CV	
AC5–neat	25	6,050	939	16	5,085	648	13	−16
	5	3,556	771	22	3,229	354	11	−9
	1	1,916	400	21	2,081	169	8	9
AC5–1.5 % CNF	25	8,489	214	3	6,352	740	12	−25
	5	5,331	760	14	4,623	265	6	−13
	1	3,048	545	18	3,460	312	9	14
AC5–6.5 % CNF	25	5,274	920	17	3,914	395	10	−26
	5	3,753	753	20	3,257	251	8	−13
	1	2,366	268	11	2,548	259	10	8

SD standard deviation, *CV* coefficient of variation

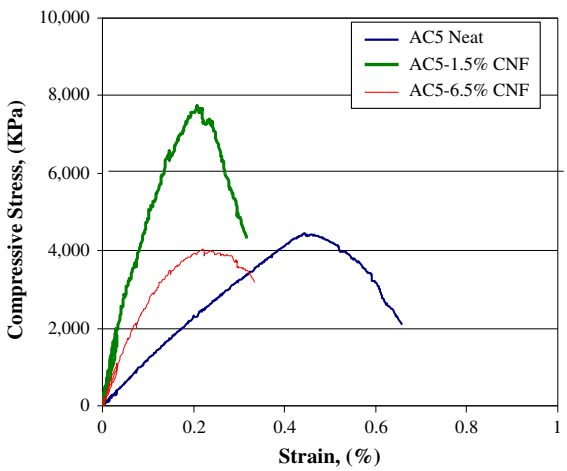

Fig. 11 Stress–strain curve as a result of uniaxial compression test DEM simulation

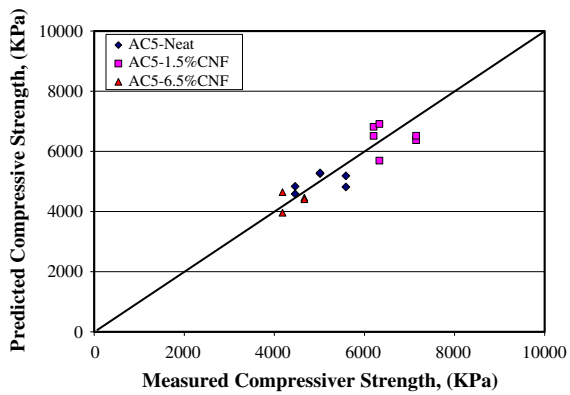

Fig. 12 Measured versus DEM simulated compressive strengths of neat and CNF modified HMA mixture

variation of the measured values for all the HMA mixtures studied.

In general, the difference in modulus and strength values could be attributed to 2D nature of the modeling with fewer particle-to-particle contacts as appose to actual 3D laboratory testing. It should be noted that the differences might also be due to the difference in test type; the actual test values are from indirect tensile test while the simulation test results are based on uniaxial compressive test. A calibration scheme needs to be developed which can facilitate improved predictions. It is believed simulation of large sized image will represent accurate shape and size distribution of HMA mixture, which can improve the predictions. However, such simulation will increase the number of particles thus increasing the simulation time. Furthermore, other factors including but not limited to the adhesion and cementatious effects, viscoelastic nature of mixtures, percentage of air voids, compaction level, and particle size distribution of aggregates can cause discrepancies in stress strain behavior. Such factors also need to be investigated.

6 Summary and conclusions

Micro-mechanical model of HMA mixtures were developed based on advanced imaging and DEM techniques. A 2D, synthetic, heterogeneous microstructure of HMA was reconstructed using scanned images of indirect tensile test specimens. The simulations were conducted using the commercially available PFC^{2D} DEM code. The developed DEM

Table 5 Summary of compressive strength test results and DEM simulation

Mix Type	Test results (KPa)			DEM simulation (KPa)			% Difference
	ICS	SD	CV (%)	S_c	SD	CV (%)	
AC5–neat	5,022	504	10	4,974	288	6	−1.0
AC5–1.5 % CNF	6,561	457	7	6,471	432	7	−1.4
AC5–6.5 % CNF	4,424	281	6	4,543	372	8	2.6

SD standard deviation, *CV* coefficient of variation

utilized elastic constitutive models to predict the stress–strain response of neat and CNF modified HMA mixtures through uniaxial virtual compressive test simulations.

It was found that the micromechanical DEM simulation accurately predicted the dynamic moduli of AM and aggregate. However, the HMA dynamic moduli using the quasi-elastic approach were under-predicted for a range of AM moduli at 25 °C. It was found that the predicted HMA dynamic modulus and compressive strength were a function of aggregate volume fraction as obtained by HMA scanned images. Correction factors were developed for aggregate volume fraction. It was observed that the moduli and strength predictions significantly improved with the application of correction factor. Nevertheless, the developed micromechanical DEM along with the empirical correction factor able to capture fairly well the mechanical behavior of HMA mixtures modified with different dosage of carbon nanofibers.

It is recommended developing improved calibration scheme, which can facilitate better predictions. Other factors such as binder aggregates adhesion, plasticity and viscoelastic effects, percentage of air voids, and compaction level, also need to be investigated. Such analysis will enhance the predictive efficiency and accuracy of the 2D image-based micromechanical model.

Acknowledgments The authors wish to express their sincere thanks to the University of Louisiana at Lafayette for using their facility and financial support. Special thanks are also extended to Mr. Mark Leblanc, laboratory assistant for assisting in experimentations.

References

1. Papagiannakis AT, Abbas A, Masad E (2002) Micromechanical analysis of viscoelastic properties of asphalt concretes. Transp Res Rec 1789:113–120
2. Dai Q, Sadd MH, You Z (2006) A micromechanical finite element model for linear and damage-coupled viscoelastic behaviour of asphalt mixture. Int J Numer Anal Meth Geomech 30(11):1135–1158
3. Collop AC, McDowell GR, Lee Y (2004) Use of the distinct element method to model the deformation behavior of an idealized asphalt mixture. Int J Pavement Eng 5(1):1–7
4. You Z (2003) Development of a micromechanical modeling approach to predict asphalt mixture stiffness using the discrete element method. Doctoral Dissertation, University of Illinois at Urbana-Champaign, Urbana
5. Buttlar WG, You Z (2001) Discrete element modeling of asphalt concrete: a micro-fabric approach. Transp Res Rec 1757:111–118
6. You Z, Buttlar WG (2005) Application of microfabric discrete element modeling techniques to preict complex modulus of asphalt–aggregate hollow cylinders subjected to internal pressure. J Transp Res Rec 1929:218–226
7. Abbas AR (2004) Simulation of the micromechanical behavior of asphalt mixtures using the discrete element method. Doctoral Dissertation, Department of Civil and Environmental Engineering Washington State University, San Jose
8. Adhikari S, You Z (2008) Distinct element modeling of the asphalt mixtures: from two-dimensional to three-dimensional models. Paper no. 08-1626, Transportation Research Board 87th Annual Meeting (CD-ROM)
9. You Z, Buttlar WG (2004) Discrete element modeling to predict the modulus of asphalt concrete mixtures. ASCE J Mater Civ Eng 16(2):140–146
10. Cundall PA (1971) A computer model for simulating progressive large scale movements in blocky rock systems. In: Proceedings of the symposium of the international society for rock mechanics, vol 1, Paper No. II-8, Nancy
11. Cundall PA, Strack ODL (1979) A discrete numerical model for granular assemblies. Géotechnique 29:47–65
12. Itasca Consulting Group (2004) ''PFC 2D Ver. 3.1,'' Minneapolis
13. Khattak MJ, Roussel C (2009) Micromechanical modeling of hot-mix asphalt mixtures by imaging and discrete element methods. J Transp Res Rec 2127:98–106
14. Liu Y, You Z (2011) Discrete-element modeling: impacts of aggregate sphericity, orientation, and angularity on creep stiffness of idealized asphalt mixtures. J Eng Mech 137(4):294–303
15. Chen j, Huang B, Chen F, Shu X (2012) Application of discrete element method to superpave gyratory compaction. Road Mater Pavement Des:480–500. doi:10.1080/14680629.2012.694160

16. Mahmoud E, Masad E, Nazarian S (2010) Discrete element analysis of the Influences of aggregate properties and internal structure on fracture in asphalt mixtures. J Mater Civ Eng 22(1):10–20
17. Khattak MJ, Kyatham V (2008) Visco-elastic modeling of lime-modified asphalt matrix and hot mix asphalt under moisture damage. J Transp Res Board, No. 2057. National Research Council, Washington D.C.
18. Kim YR, Momen M, King M (2005) Report No. FHWA/NC/2005-03 typical dynamic moduli for north carolina asphalt concrete mixtures. Final Report, FHWA
19. Murrell SAF (1958) The strength of coal under triaxial compression. In: Walton WH (ed) Mechanical properties of non-metallic brittle materials. Butterworths, London, pp 123–145
20. Griffith AA (1921) The phenomena of rupture and flow in solids. Phil Trans R Soc (London) A 221:163–198
21. Griffith AA (1925) Theory of rupture. In: Proceedings of the 1st congress of applied mechanics. Technische Bockhandel en Drukkerij, Delft, 1924, pp 55–63
22. McClintock FA, Walsh JB (1967) Friction on Griffith cracks under pressure. In: Proceedings of the 4th U.S. Congress of Applied Mathematics, Berkeley, pp 1015–1021